Analysis of the Coriolis perturbed rovibrational spectrum of the C-O asymmetric stretch and C-C symmetric stretch of trimethylene oxide

Omar Mahassneh and Jennifer van Wijngaarden*

Department of Chemistry, University of Manitoba, Winnipeg Manitoba, R3T 2N2 Canada

*Corresponding author

Email: vanwijng@cc.umanitoba.ca

Phone: (204)474-8379

Fax: (204)474-7608

Research highlights

-High resolution infrared spectra of trimethylene oxide (oxetane) recorded with synchrotron light

-Dense spectrum due to hotbands involving low-lying ring puckering states

-C-O asymmetric (ν_{23}) and C-C symmetric (ν_6) stretches rovibrationally analyzed

-Coriolis interactions treated in global fit of three interacting states

Abstract

Rotationally-resolved vibrational spectra of trimethylene oxide (c-C_3H_6O) were recorded using synchrotron radiation from the Canadian Light Source between 400 and 1200 cm^{-1} with a resolution of 0.000959 cm^{-1}. The dense spectra are composed of transitions arising from excitation of several fundamental vibrations as well as hotbands and combination bands involving the very low frequency ring puckering (ν_{18}) vibration at ~53 cm^{-1}. To date, 3452 transitions have been assigned corresponding to the C-O asymmetric stretch (ν_{23}) at ~1008 cm^{-1} and the C-C symmetric stretch (ν_6) at ~1033 cm^{-1} which are coupled via second order c-type Coriolis interaction. An additional perturbation from a lower energy state was observed and attributed to a first order b-type interaction with a state that is likely the combination of the C-C asymmetric stretching (ν_{24}) at ~937 cm^{-1} and ring puckering motions. An additional 916 transitions involving the C-O stretching mode were assigned to two hotbands that originate in the first and second excited ring puckering states of trimethylene oxide. Accurate band centers for the ν_6, ν_{23}, $\nu_{23}+\nu_{18}$, $\nu_{23}+2\nu_{18}$ and $\nu_{24}+\nu_{18}$ vibrational states were determined and are compared with harmonic and anharmonic frequency estimates at the MP2 and DFT B3LYP levels using the 6-311++G(d,p) basis set. The analysis of additional features at lower frequency is in progress and will be reported in a subsequent article.

1. Introduction

Small heterocycles such as trimethylene oxide (TMO, c-C_3H_6O)), also known as oxetane, are interesting vehicles for exploring the connection between the unique spectroscopic signature of a molecule and its underlying potential energy surface.[1,2] In four-membered rings, the backbone geometry is governed by balancing two opposing effects: the classical ring strain which favours planarity and the preference for staggered C-H bonds which favours a puckered geometry. Gwinn and co-workers, in a series of papers that employed data in the microwave and far infrared region,[3–5] showed that the potential energy surface of TMO is quartic along the ring displacement coordinate and possesses a small barrier (15.3(4) cm^{-1})[6] to planarity which lies below the zero point energy of the molecule. Thus, while the equilibrium structure of TMO is puckered, the ground state ring geometry is best described as quasiplanar as a result of the barrierless large amplitude ring puckering motion. This led to extensive spectroscopic studies of related four-membered heterocycles such as trimethylene sulfide (TMS) and silacyclobutane (SCB) in which substitution by larger atoms (S and Si, respectively) induce important changes in the underlying potential energy surface. In both cases, the barriers to planarity (274.2(2) cm^{-1} (TMS)[7]; 440(3) cm^{-1} (SCB)[8]) are considerably higher and give rise to inversion tunnelling features in the microwave and far infrared spectra.[7,9–14]

TMO has been the subject of numerous spectroscopic studies in the microwave,[3,4,15,16] millimeterwave,[17] far infrared[5,6,18–20] and infrared regions.[21–27] These investigations have largely focused on the ground and ring puckering vibrational states. Such low frequency motions are often difficult to model when the underlying potential is

anharmonic although a number of theoretical studies on TMO have been reported.[28–30] The shallow double-well potential of TMO gives rise to irregularly spaced energy levels[5] for the ring puckering states. The Q branches that correspond to excitation of quanta of ring puckering have been assigned up to the v_{rp}=10-11 hotband by Jokisaari and Kaupinnen[6] and the band centers confirm this uneven energy level spacing. Most notable in this regard is the unusually large gap between the fundamental (52.90(5) cm^{-1}) and first hotband (89.56(5) cm^{-1}) in the far infrared spectrum. At room temperature, the Boltzmann population of the excited ring puckering states is appreciable with the first five excited states lying within 6 kJ/mol of the ground state.[20] Consequently, the observed vibrational spectra of TMO at higher frequencies will also contain contributions from hotbands that originate in these low-lying ring puckering levels.[22,24] The spectral complexity that results from such a high density of states makes the analysis of bands incredibly challenging and in this regard, rotationally-resolved IR data is valuable as it would enable irrefutable assignment of the fundamental vibrations and hotbands of TMO. To date, only spectra of the ring puckering fundamental and its first four hotbands have been rotationally analyzed by Winnewisser and co-workers.[19,20] Their accurate spectroscopic constants establish a solid foundation for investigating the remaining vibrational modes of TMO via high resolution infrared spectroscopy.

In this article, we report the analysis of the high resolution rovibrational spectrum of TMO in the 960-1060 cm^{-1} region using data collected at Canada's national synchrotron facility. This is the first rotationally resolved investigation of the vibrations of this molecule beyond the ring puckering mode. The modes of interest in this region are the intense C-O asymmetric stretch (v_{23}) and the less intense features of the C-C symmetric (v_6) and

asymmetric (ν_{24}) stretches and hotbands originating in excited ring puckering (ν_{18}, $2\nu_{18}$) states. Our analysis indicates the presence of Coriolis interactions due to the high density of states in this region. The experimental results are complemented by quantum chemical predictions of the band centers using MP2 and DFT theory which provide excellent estimates of the vibrational frequencies in this region and also identify a few inconsistencies in the original assignment of the fundamental bands of TMO.[26] The spectroscopic constants determined for these modes, from band centers to the rotational and the centrifugal distortion constants, provide critical benchmarks for future experimental and theoretical studies of floppy molecules such as TMO.

2. Experimental details

The rotationally resolved infrared spectrum of TMO was collected at the Canadian Light Source (CLS) far infrared beamline using a Bruker IFS125 HR spectrometer capable of collecting spectra with an unapodized resolution of 0.000959 cm^{-1}. Such high spectral resolution requires the inclusion of a small entrance iris (1 mm diameter) and synchrotron radiation (SR), a highly collimated light source, offers a clear advantage over conventional thermal light sources in this respect.[31] It has been shown that the 'synchrotron advantage' in the far infrared region leads to an improvement in signal-to-noise of about one order of magnitude over a mercury lamp or globar.[32] A sample of liquid TMO was purchased from Sigma Aldrich Canada and the vapour was used to fill a 2 m multipass cell at room temperature. Spectra were subsequently recorded between 400 and 1200 cm^{-1} using a KBr beamsplitter and GeCu detector at pressures ranging from 5 to 180 mTorr in order to observe bands of both high and low intensity. The calculated Doppler linewidth of TMO

in this region is such that the observed linewidths (FWHM) are instrument limited. Background interferograms were collected at lower resolution (0.01536 cm^{-1}) and transformed with appropriate zero filling before calculation of the absorption spectrum.

3. Frequency calculations

Vibrational frequencies of TMO were estimated at the MP2 and DFT/B3LYP levels of theory with a 6-311++G(d,p) basis set using optimized geometries in Gaussian 09.[33] Anharmonic corrections were also computed via second order perturbation analysis as reported for other four-membered rings 2-oxetanone[34] and 3-oxetanone.[35] The calculated frequencies for TMO are listed in Table 1 along with descriptions of the corresponding motions. The band numbers follow the convention established by Kydd *et al.*[26] and the symmetry labels used are correlated to those based on C$_{2v}$ symmetry.

4. Spectral assignment and analysis

The equilibrium structure of TMO at the MP2/6-311++G(2d,2p) level is predicted to be puckered with C$_s$ symmetry but as the barrier to planarity is below the zero point energy, the ground state structure is pseudoplanar with C$_{2v}$ symmetry. Although the IR spectra collected at the CLS extend from 400 cm^{-1} to 1200 cm^{-1}, the current study focuses on the spectral features surrounding the C-O asymmetric stretch at 1008 cm^{-1} as this band appeared well-isolated from others as shown in Figure 1. The nuclear spin statistical weights of TMO have been detailed by Winnewisser *et al.*[19] in their study on the ν_{18} ring puckering mode. Using molecular symmetry group theory, the symmetry of the nuclear spin part of the wavefunction under C$_{2v}$(M) is represented by: $\Gamma_{ns} = 24A_1 \oplus 12A_2 \oplus$

$16B_1 \oplus 12B_2$ which means that ground state rotational energy levels with A_1/A_2 (ee/eo) symmetry have spin weight 28 and those with B_1/B_2 (oo/oe) symmetry have spin weight 36 (where e=even, o=odd parity of K_a and K_c). These weights (and those of excited rovibrational levels), being similar, did not lead to significant alternation in the intensity of transitions in the rovibrational patterns.

Table 1: Predicted vibrational frequencies (cm^{-1}) of TMO compared with previously reported experimental values in the gas phase unless otherwise noted.

			Expt[a]	MP2 /6-311++(d,p)		B3LYP /6-311++(d,p)		
				harmonic	anharmonic	harmonic	scaled[d]	anharmonic
A_1	1	β-CH-sym stretch	2979	3125	3044	3072	2973	2910
	2	α-CH-sym stretch	2894	3076	2959	3026	2928	2850
	3	α-CH$_2$-scissor	1505	1559	1502	1540	1491	1486
	4	β-CH$_2$-scissor	1452	1507	1486	1495	1447	1478
	5	α-CH$_2$-wag	1343	1395	1343	1374	1330	1340
	6	CC-sym stretch	1033	1071	1046	1040	1007	1021
	7	CO-sym stretch	909	944	883	920	890	898
	8	Ring deformation	(785)*	868	841	815	789	778
A_2	9	α-CH-asym stretch		3147	3006	3061	2962	2902
	10	β-CH$_2$-twisting	1183[b]	1230	1202	1234	1194	1195
	11	α-CH$_2$-twist		1176	1150	1159	1122	1134
	12	α-CH$_2$-rock	842[b]	847	834	839	812	832
B_1	13	β-CH-asym stretch	3006	3199	3057	3123	3023	2979
	14	α-CH-sym stretch	2938	3148	3004	3059	2961	2901
	15	α-CH$_2$-twist	1137	1223	1188	1196	1158	1169
	16	α-CH$_2$-rock	(840)*	1175	1149	1147	1110	1130
	17	β-CH$_2$-rock	703	714	714	770	745	756
	18	Ring pucker	53[c]	133	83	66	64	99
B_2	19	α-CH-asym stretch	2887	3070	2926	3017	2920	2854
	20	α-CH$_2$-scissor	1480	1531	1566	1514	1465	1474
	21	α-CH$_2$-wag	1289	1335	1301	1319	1277	1283
	22	β-CH$_2$-wag	1230	1275	1244	1265	1224	1228
	23	CO-asym stretch	1008	1044	1015	1023	990	989
	24	CC-asym stretch	937	970	950	942	912	904

[a]Ref 26; [b]From Raman spectrum of liquid; [c]Ref 19; [d]Scaled by 0.9679 as per ref 38. *Mis-assigned in ref 26: ν_8 band was observed at 839 cm^{-1} in this work (previously assigned to ν_{16}); feature reported at 785 cm^{-1} in ref 26 corresponds to $\nu_{17}+\nu_{18}$ (this work).

4.1 Preliminary assignment of the v_{23} band

The C-O asymmetric stretching mode (v_{23}) has the largest IR intensity outside of the C-H stretching region above 2800 cm^{-1}. The vibrational motion has B$_2$ symmetry and thus the rovibrational transitions follow *b*-type selection rules. Upon initial inspection, there were clear rotational patterns visible in the P and R branches. Based on a visual estimate of the band center and using the ground state rotational constants previously reported,[20] the spectrum was simulated to better understand the observed patterns including the nuclear spin statistical weights. A Loomis-Wood plot was then constructed using the
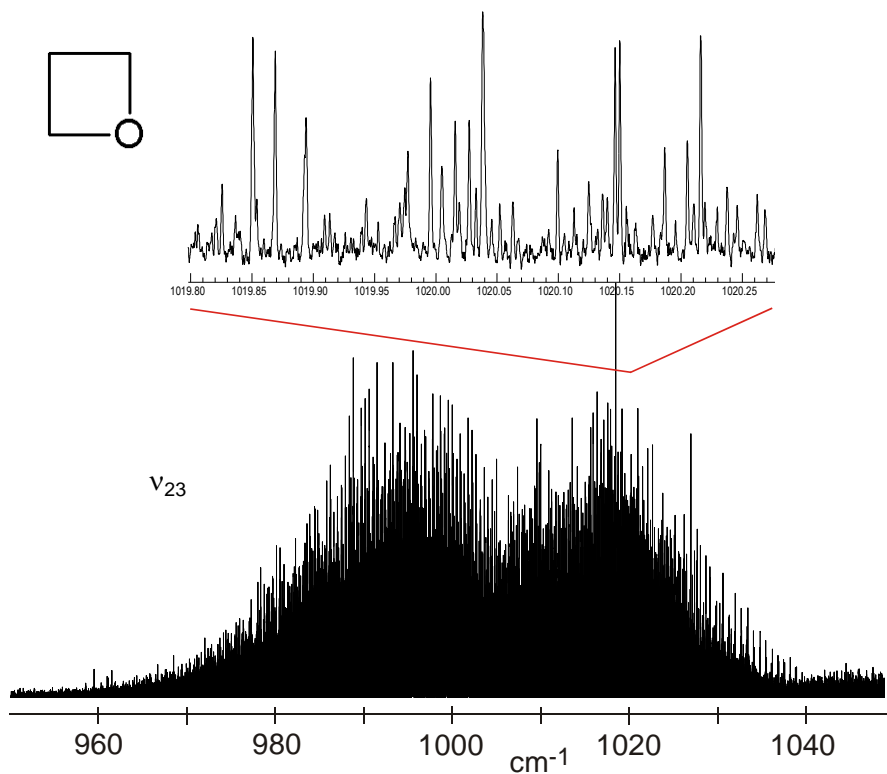

Figure 1. C-O asymmetric stretch (v_{23}) of TMO collected with 5 mTorr of vapour. Inset highlights the rovibrational structure over 0.5 cm^{-1}.

interactive add-in for Igor Pro[36] and used to identify the leading lines in the most intense progressions. A portion of the Loomis-Wood plot of the R-branch is shown in Figure 2. The assignment of these first sets of transitions to appropriate quantum numbers was confirmed using ground state combination differences. After several progressions were assigned and fit using Watson's A-reduced Hamiltonian, I^r-representation in Pickett's SPFIT program,[37] the simulated spectrum was refined and the process continued in an iterative fashion until over 1000 of the most intense transitions were assigned. This was done with the ground state constants fixed to those established by Moruzzi *et al.*[20] from analysis of the ν_{18} ring puckering mode using the same Hamiltonian. While the preliminary fit was satisfactory with rms error of only 0.000213 cm^{-1}, the constants did not account for all observed transitions. As shown in Figure 2, the strong progressions in the Loomis-Wood
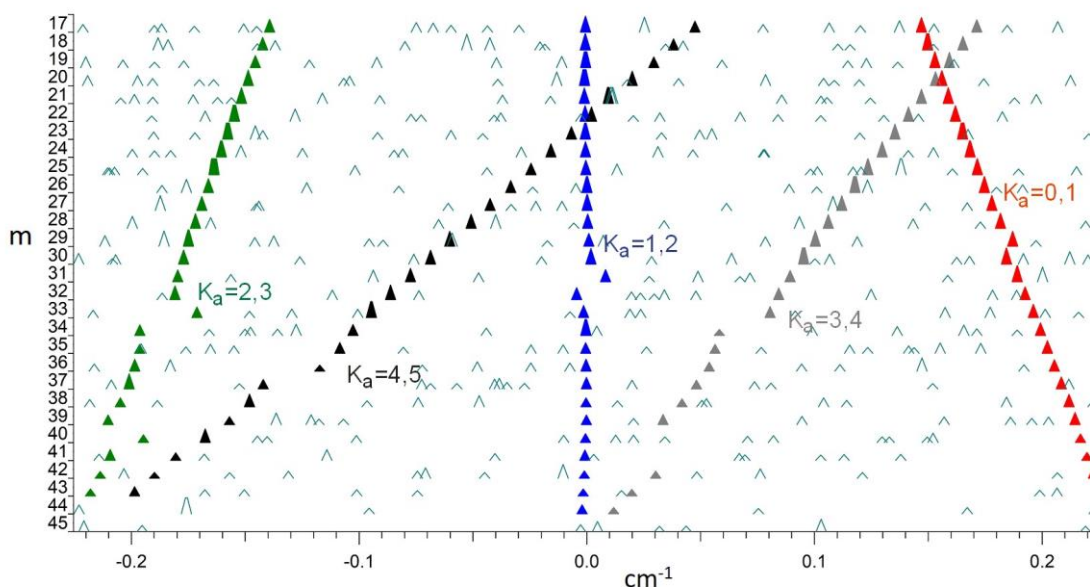

Figure 2. A portion of the Loomis-Wood plot of the R-branch of the C-O asymmetric stretching band (ν_{23}) of TMO. The onset of a perturbation in the K_a=0,1 progression is observed here at m=29 (appearing at m=31 in K_a=1,2 and higher m in subsequent progressions). A second perturbation is observed in the K_a=2,3 progression (also appearing at higher m in subsequent progressions).

plot revealed the presence of a perturbation around J=29 in the K_a=0,1 series (and at higher J values for subsequent K_a series). A second perturbation is seen for the higher K_a progressions starting with K_a=2,3 around J=38 (and at higher J values for subsequent K_a series). In order to fit these shifted transitions in the v_{23} band, a global analysis of this and its interacting states is needed.

4.2 Assignment of hotbands

Inspection of the Loomis-Wood plot in Figure 2 reveals additional progressions belonging to another *b-type* band other than v_{23}. As no other *b*-type fundamentals are predicted in this region, the most likely candidate was determined to be a hotband originating in the first ring puckering vibrational level (v_{18}) at ~53 cm^{-1}. Based on C_{2v} symmetry, the v_{18} vibration has B_1 symmetry while the coupled state between this and the C-O asymmetric stretch, $v_{18}+v_{23}$, has the symmetry of $B_1 \otimes B_2 = A_2$. Since the direct product of the irreproducible representations of the initial (B_1) and the final (A_2) vibrational state wavefunctions and of the b-dipole component (B_2) is totally symmetric, the assigned features are consistent with an IR active hotband of type: $v_{18}+v_{23}-v_{18}$ which is centered around 1002 cm^{-1}. Transitions with quantum number J values ranging from 5 to 31 and values of K_a up to 14 in the P-branch and R-branch were subsequently assigned using lower state combination differences from the v_{18} state[20] as an added check. The rovibrational transitions were fit using Watson's A-reduced Hamiltonian, I^r-representation with the lower state constants fixed to those for the v_{18} ring puckering state. The rms error of 0.000323 cm^{-1} was satisfactory and the results are summarized in Table 2.

Table 2: Spectroscopic constants (cm^{-1}) determined from fitting the first two hotbands of the ν_{23} mode of TMO that originate in excited ring puckering states (ν_{18}, $2\nu_{18}$).[a]

	ν_{18}[a]	$\nu_{18} + \nu_{23}$	$2\nu_{18}$[a]	$2\nu_{18} + \nu_{23}$
G_v	52.920348	1054.448596(52)	142.579784	1141.344073(60)
Rotational Constants				
A	0.402209858	0.4022555(99)	0.402243871	0.4008564(93)
B	0.391155554	0.3897205(87)	0.390900214	0.3895381(84)
C	0.22589666	0.22620928(28)	0.22645821	0.22635724(42)
Quartic Centrifugal Distortion Constants ($\times 10^8$)				
Δ_J	16.6282	18.261(32)	16.127	13.506(58)
Δ_{JK}	-21.5803	-32.38(21)	-15.11	-52.15(50)
Δ_K	32.248	91.42(33)	26.168	83.89(65)
δ_j	5.3811	5.3811	5.5755	5.5755
δ_k	5.9528	5.9528	3.223	3.223
Sextic Centrifugal Distortion Constants ($\times 10^{12}$)				
Φ_J	0.537	0.537	4.87	4.87
Φ_{JK}	-1.79	-1.79	-0.2	-0.2
Φ_{KJ}	1.93	1.93	-3.3	-3.3
Φ_K	-0.397	-0.397	2.1	2.1
φ_j	0.097	0.097	0.83	0.83
φ_{jk}	0.54	0.54	-0.47	-0.47
φ_k	0.871	0.871	9.94	9.94
# lines		516		402
rms error		[0.000323]		[0.000215]

[a]Ref 20. Values in gray fixed to the lower state parameter.

Additional progressions remained in the Loomis-Wood plot and were soon attributed to another hotband centered at 999 cm^{-1}. The band follows *b-type* selection rules and using the spectroscopic constants for the second excited ring puckering state ($2\nu_{18}$) at 154 cm^{-1} reported by Moruzzi *et al.*,[20] the features were assigned to the second hotband: $2\nu_{18}+\nu_{23}-2\nu_{18}$. Symmetry confirms that this band is *b*-type as the irreducible representations of the initial state ($B_1 \otimes B_1 = A_1$), final state ($B_1 \otimes B_1 \otimes B_2 = B_2$) and b-dipole components (B_2) combine to give A_1 symmetry. Progressions of rovibrational transitions with the quantum number J values ranging between J=6 and J=28 and K_a values up to 15 in the P-branch and R-branch were identified and fit as described for the previous hotband. The rms

error value of this fit of 402 transitions was 0.000215 cm^{-1} and the results are provided in Table 2.

Figure 3 shows a portion of the dense spectrum arising from transitions related to the C-O asymmetric stretch (ν_{23}) and the hotbands involving quanta of ring puckering (ν_{18}). While there was good correspondence between the simulated and experimental spectrum for roughly 2000 of the most intense lines in these three bands, a number of transitions in the fundamental band were noticeably shifted as first noted in the Loomis-Wood plot in Figure 2. Fortunately, the ground state and ν_{18} energy levels were well-characterized in the literature which allowed us to focus on potential perturbations to the upper states.
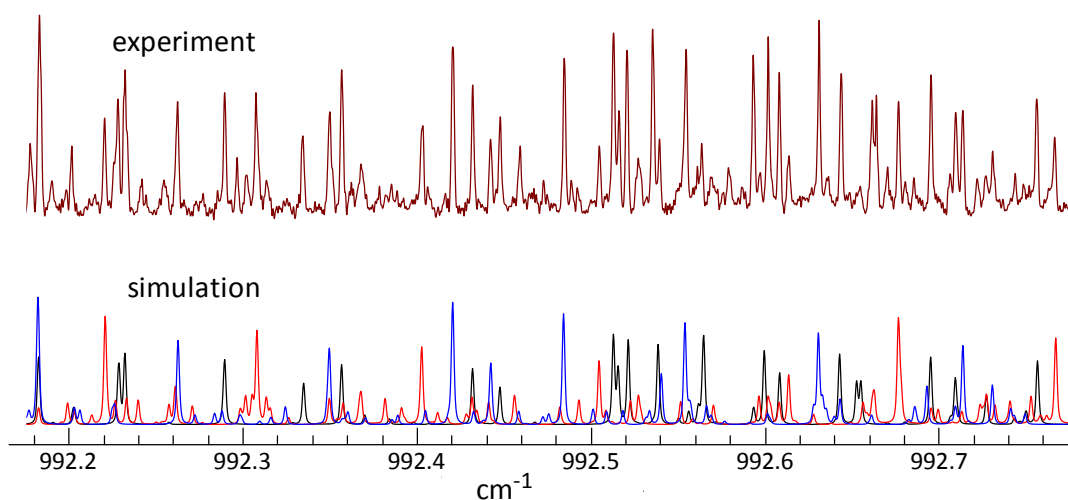

Figure 3. Top: A portion of the experimental P-branch spectrum involving the C-O asymmetric stretch (ν_{23}) of TMO. Bottom: The simulated transitions are those of the ν_{23} fundamental (black), the first hotband $\nu_{18}+\nu_{23}-\nu_{18}$ (red) and second hotband $2\nu_{18}+\nu_{23}-2\nu_{18}$ (blue).

4.3 Coriolis interactions

The obvious candidates for Coriolis interaction with the energy levels of the ν_{23} (B$_2$) band are those from the nearby ν_6 state at 1033 cm^{-1} which corresponds to the C-C

13

symmetric stretch (A_1) of TMO. As the IR intensity of this vibration is lower, the pressure of TMO in the cell was increased to 180 mTorr in order to collect the spectrum of the ν_6 R-branch shown in Figure 4. Its P-branch is buried by the saturated spectrum of the lower frequency ν_{23} mode. Despite these difficulties, the *a-type* ν_6 band was partially analyzed with the help of a Loomis-Wood plot. The patterns in the ν_6 spectral region revealed the onset of a noticeable perturbation at J=37 for the K_a=(0, 1) progression (and at higher J for the higher K_a values). To visualize the energy levels involved, preliminary sets of spectroscopic parameters from the initial fits of the ν_{23} and ν_6 bands were used to generate a reduced energy plot as show in Figure 5. From the progressions plotted, the K_a=0,1 levels in the ν_6 state cross those of K_a=2,3 of the ν_{23} state at J=37. The energy levels involved
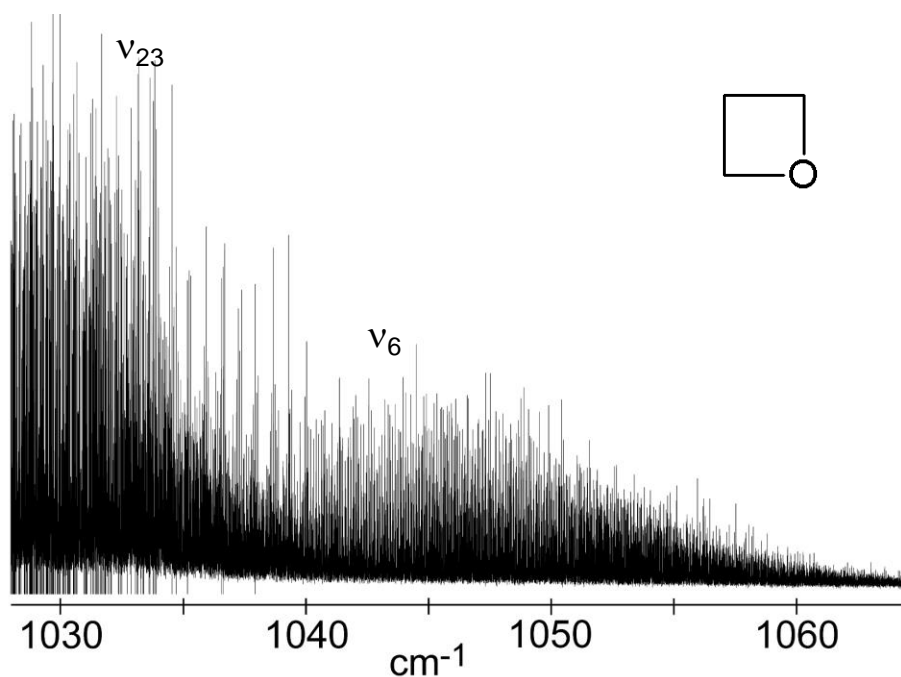

Figure 4. C-C symmetric stretch (ν_6) of TMO collected with 180 mTorr of vapour. The spectrum of the ν_{23} band (left) is saturated under these conditions.
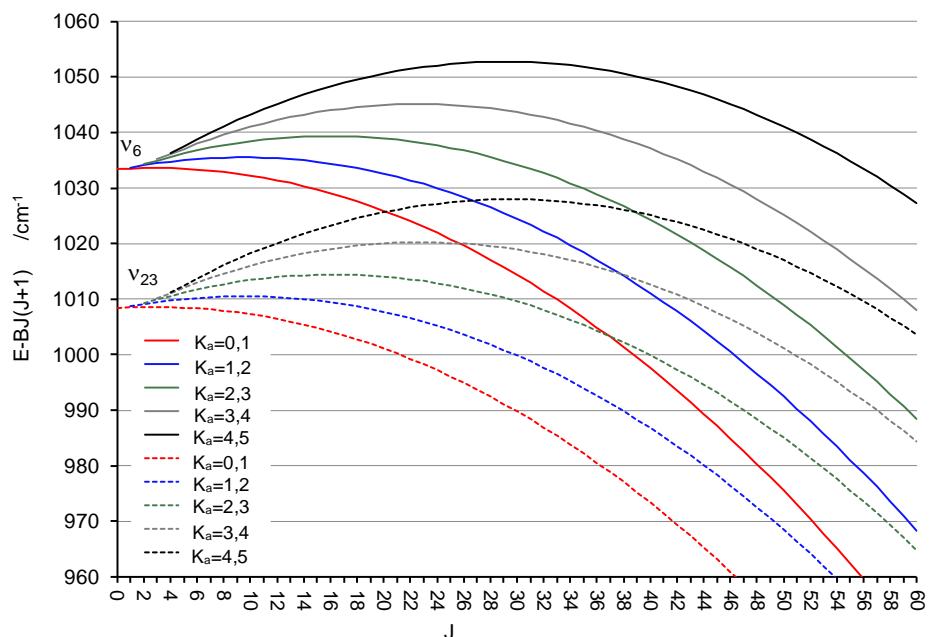
Figure 5. Reduced energy plot showing the overlap of energy levels of the ν_6 and ν_{23} vibrational states of TMO originating at 1033 cm^{-1} and 1008 cm^{-1}, respectively. The K_a=0,1 progression of the former crosses the K_a=2,3 progression of the latter at J=38 with subsequent progressions crossing at higher J levels.

have the correct symmetry for a *c-type* Coriolis interaction and based on the affected progressions in Figure 5, this was determined to be second order. When the Coriolis coupling constant F_{ab} (the co-efficient of the ($J_aJ_b+J_bJ_a$) term in the Hamiltonian) was included in a simultaneous fit of these two bands, it allowed the assignment of 926 additional transitions in the ν_6 band and 296 additional transitions in the ν_{23} band. The simultaneous fit of 2474 transitions yielded an estimate of the Coriolis coupling constant F_{ab} (ν_{23},ν_6) and provided refined spectroscopic parameters for each of these fundamentals. This constant seems sufficient to address the effects of the second perturbation noted in Figure 2 that emerges in the K_a=2,3 progression at higher J values.

The remaining perturbation of the ν_{23} band in Figure 2 must arise from interactions with a lower frequency band in order for the K_a=0,1 energy levels in Figure 5 to be affected.

15

The nearest band observed to the red of the C-O asymmetric stretch at 1008 cm^{-1} corresponds to the ν_7 C-O symmetric stretch near ~908 cm^{-1} which was visible even at 5 mTorr along with a hotband at ~864 cm^{-1}. As *c-type* Coriolis interactions are allowed by symmetry between the ν_7 and ν_{23} states, a preliminary analysis was conducted to establish the spectroscopic constants of these two bands. Although over 2000 lines were included in the fit, a perturbation in the hotband ($\nu_7+\nu_{18}-\nu_{18}$) was not addressed and thus, a more accurate analysis will be presented in a subsequent article. For the present work, this preliminary analysis was sufficient to estimate the energies of rovibrational levels of the ν_7 and $\nu_7+\nu_{18}$ states which originate at 908.42725(3) cm^{-1} and 916.85974(3) cm^{-1}, respectively for comparison with those of the ν_{23} band. This revealed that neither of these states were close enough in energy to account for the onset of a perturbation in the ν_{23} spectrum in the lowest K_a progressions starting around J=27.

According to the quantum chemical calculations, a more likely candidate for interaction is the ν_{24} C-C asymmetric stretch at 956 cm^{-1}(harmonic)/940 cm^{-1}(anharmonic) (MP2/6-311++G(d,p)). This band has very low infrared intensity and was not observed in this work but the band center was reported in a low resolution study in the gas phase by Kydd *et al.* at 937 cm^{-1}.[26] This vibration has B_2 symmetry and thus, no Coriolis interaction is allowed between this and the ν_{23} vibration. The $\nu_{18}+\nu_{24}-\nu_{18}$ hotband, however, is a potential candidate by symmetry as the direct product of the $\nu_{18}+\nu_{24}$ and ν_{23} vibrational state symmetries $A_2 \otimes B_2 = B_1$ permits *b-type* Coriolis interactions. Unfortunately, no experimental spectroscopic parameters could be determined for the $\nu_{18}+\nu_{24}-\nu_{18}$ band as it was not observed even in the higher pressure scans at 180 mTorr. Thus, an approximation was needed. The rotational and centrifugal distortion constants from the above-analyzed
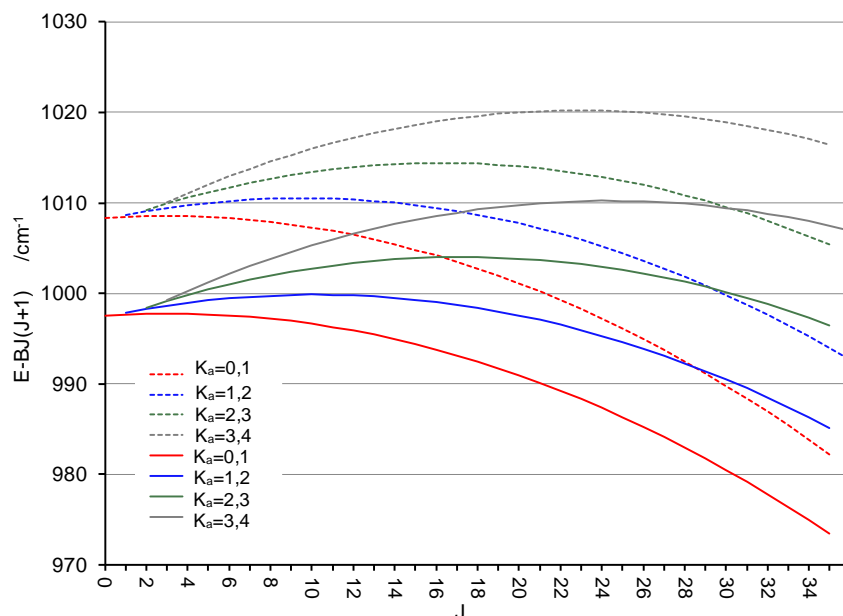
Figure 6. Reduced energy plot of TMO showing the overlap of energy levels of the ν_{23} vibrational state and a "dark" state (proposed to be $\nu_{18}+\nu_{24}$) originating at 1008 cm^{-1} and 997 cm^{-1}, respectively. The $K_a=0,1$ progression of the former crosses the $K_a=1,2$ progression of the latter at J=29 with subsequent progressions crossing at higher J levels.

$\nu_{18}+\nu_{23}$ state (another combination state of similar energy and symmetry) were used to predict the rotational spacing of the energy levels in the $\nu_{18}+\nu_{24}$ "dark" state. Various values of the band center were tested that were consistent with coupling the ν_{24} (937 cm^{-1}) and ν_{18} (53 cm^{-1}) modes to explain perturbations seen in the ν_{23} band. In Figure 6, for example, a reduced energy plot for this "dark" state originating at ~997 cm^{-1} crossed the $K_a=0,1$ levels of the ν_{23} band at J=27 and is consistent with a first order b-type Coriolis interaction.

When the first order Coriolis coupling constant G_b (the coefficient of iJ_b in the Hamiltonian) was included in a simultaneous fit of the three bands ν_{23}, ν_6 and $\nu_{18}+\nu_{24}-\nu_{18}$, it allowed the assignment of more than a thousand additional transitions in the ν_{23} band. In the end, 2328 rovibrational transitions in the ν_{23} band with values of the quantum number J extending from 4 through 51 and values K_a up to 28 were fit. The spectroscopic constants

for the global fit of 3452 transitions using Watson's A-reduced Hamiltonian in the I^r representation are shown in Table 3. The rms error of 0.000221 cm^{-1} is consistent with those of other bands analyzed for this molecule. Only the band origin of $\nu_{18}+\nu_{24}-\nu_{18}$ and the Coriolis coupling constant G_b between the ν_{23} and $\nu_{18}+\nu_{24}$ vibrational states could be determined for the lower state as no rovibrational transitions could be assigned for this hot combination band.

5. Discussion

The earlier low resolution IR study[26] of TMO provided a useful survey of the approximate frequencies, selection rules and intensities of the fundamental vibrations of this molecule. This guided our high resolution work in the infrared region along with the results from quantum chemical calculations. Although only seven fundamental vibrations are expected in the recorded frequency range between 400 cm^{-1} and 1200 cm^{-1}, at least 20 band centers were observed due to excitation of hotbands and combination bands resulting in a very congested spectrum particularly between 700 cm^{-1} and 950 cm^{-1}. Preliminary assignments were made for the main features in this region including a combination band of $\nu_{17}+\nu_{18}$ at 754 cm^{-1} (not previously reported) and three hotbands of this involving excited states of the low frequency ring puckering (ν_{18}) mode starting at 785 cm^{-1} (previously mis-assigned as the ν_8 ring deformation).[26] Preliminary analysis was also completed for the actual ν_8 mode at 840 cm^{-1} (previously mis-assigned to the ν_{16} mode)[26] as well as for the ν_7 C-O symmetric stretching at 909 cm^{-1}. Each band consisted of thousands of well-

Table 3: Spectroscopic constants (cm^{-1}) determined from global analysis of transitions of the ν_6, ν_{23} modes of TMO including interactions with a "dark" state tentatively assigned as $\nu_{18}+\nu_{24}$.

	G.S.[a]	ν_{18}[a]	$\nu_{18}+\nu_{24}$	ν_{23}	ν_6
G_v	0	52.920348	997.54543(68)	1008.364520(19)	1033.405418(28)
Rotational Constants					
A	0.40179332	0.402209858	0.4022555	0.40033830(72)	0.4006200(11)
B	0.391405984	0.391155554	0.3897205	0.39010458(60)	0.3903015(10)
C	0.224510678	0.22589666	0.22620929	0.224581154(50)	0.224064344(58)
Quartic Centrifugal Distortion Constants ($\times 10^8$)					
Δ_J	16.5254	16.6282	18.261	17.1122(23)	16.1298(23)
Δ_{JK}	-4.68	-21.5803	-32.39	-2.894(16)	-2.757(16)
Δ_K	15.23	32.248	91.42	8.032(29)	13.240(30)
δ_j	5.4815	5.3811	5.3811	5.4815	5.4815
δ_k	-2.779	5.9528	5.9528	-2.779	-2.779
Sextic Centrifugal Distortion Constants ($\times 10^{12}$)					
Φ_J	0.627	0.537	0.537	0.627	0.627
Φ_{JK}	0.800	-1.79	-1.79	0.800	0.800
Φ_{KJ}	1.236	1.93	1.93	1.236	1.236
Φ_K	-2.2	-0.397	-0.397	-2.2	-2.2
φ_j	0.10	0.097	0.097	0.10	0.10
φ_{jk}	-0.897	0.54	0.54	-0.897	-0.897
φ_k	-0.19	0.871	0.871	-0.19	-0.19
Coriolis Interaction constants					
$G_b\,(\nu_{18}+\nu_{24},\,\nu_{23})$			$-6.5115(93) \times 10^{-3}$		
$F_{ab}\,(\nu_{23},\nu_6)$				$-9.6593(15) \times 10^{-4}$	
rms error				0.000221	
# lines				2328	1124

[a]Ref 20. Values in gray fixed to the lower state parameter.

resolved lines, and for most, several hundred transitions were included in a least squares fit to confirm the identity of the vibration based on selection rules and lower state combination differences. A detailed rovibrational analysis is under way including treatment of multiple perturbations which arise due to the high density of states as modes couple to
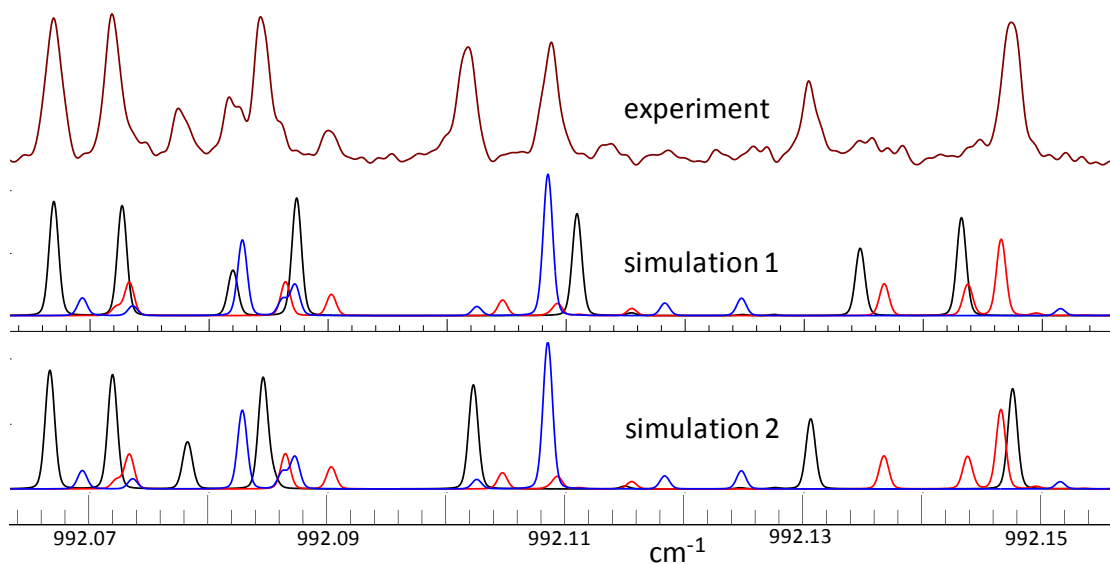
Figure 7. Top: A portion of the experimental P-branch spectrum involving the C-O asymmetric stretch (ν_{23}) of TMO. Bottom: The simulated transitions are those of the ν_{23} fundamental (black), the first hotband $\nu_{18}+\nu_{23}-\nu_{18}$ (red) and second hotband $2\nu_{18}+\nu_{23}-2\nu_{18}$ (blue). Simulations 1 and 2 refer to the calculated spectrum without and with the inclusion of the Coriolis interaction terms affecting the ν_{23} fundamental band (black), respectively.

quanta of ring puckering. In the present study, we chose to focus on a less congested spectral region to establish the quality of fit that may be achieved once interactions are treated.

For the perturbed ν_{23} C-O asymmetric stretch at 1008 cm^{-1}, the simultaneous fit of over 3400 infrared transitions with low rms error of 0.000221 cm^{-1} suggests that the model Hamiltonian employed provides a good description of the ν_{23} energy manifold and its interacting states. This result was particularly encouraging given the lack of information of the lower perturbing state which we have tentatively assigned as $\nu_{18}+\nu_{24}$ at 997.54543(68) cm^{-1}. Figure 7 shows a segment of the high resolution infrared spectrum of TMO in which some perturbed rovibrational transitions in the ν_{23} band are compared to simulations without the Coriolis interaction terms (simulation 1) and with both F_{ab} and G_b terms included (simulation 2) in the model Hamiltonian. We tested other interaction constants

and found that G_a (assuming first order *a*-type Coriolis perturbation) gave a similar numerical result and quality of fit as G_b but this assumes that the lower energy states has B_1 vibrational symmetry. Considering the symmetry and energy of the fundamental bands listed in Table 1 and possible combination bands ($\nu_7+\nu_{18}$, $\nu_7+3\nu_{18}$), no plausible candidates were identified. To confirm our present assignment, the spectrum of the $\nu_{18}+\nu_{24}-\nu_{18}$ band is needed and as this follows *b*-type selection rules, no central Q branch will be observed to aid in its identification. As the ν_{24} fundamental itself has an estimated IR intensity of only 3-6% that of the overlapping ν_{23} band (MP2 and B3LYP/6-311++(d,p)), it is clear from Figure 1 that direct measurement of this hotband (which will have even lower intensity) is not feasible.

For the hotbands of ν_{23}, the spectroscopic constants presented in Table 2 provide a reasonable fit for the assigned transitions over a range of quantum numbers. Nonetheless, these constants, in particular Δ_K, are best viewed as effective parameters as they vary quite substantially from the values observed for other vibrational states of TMO. This is likely the result of minor perturbations that have not been explicitly treated. We attempted to isolate perturbed transitions by fixing Δ_K for the upper state to the value from the lower state (either ν_{18} or $2\nu_{18}$) but the residuals (obs-calc) were poor for many of the higher K_a transitions (starting around K_a=4,5) in this case. When transitions were removed from the fit to reduce the rms error, the remaining spectroscopic parameters were not well-determined. In the end, we are confident in the assignment of transitions for both hotbands as we used lower state combination differences for confirmation but without a clear idea of which transitions are affected (from noticeable shifts in the Loomis-Wood plot for example which is typical for localized interactions), minor perturbations are difficult to

address. We also note that the unusually large Δ_K constants for the $\nu_{23}+\nu_{18}$ and $\nu_{23}+2\nu_{18}$ states in Table 2 may also be a consequence of a vibrational dependence. For the excited ring puckering states of TMO themselves, previous studies in the microwave[15] and millimeterwave[17] range have investigated the effect of the double well potential on quartic centrifugal distortion constants. Table 3, for example, shows that the Δ_K constant in the ν_{18} state is double that of the ground state.[20]

The band origins of the ν_6 (1033.405418(28) cm^{-1}) and ν_{23} (1008.364520(19) cm^{-1}) fundamental vibrations have been accurately determined. These values compare well with the quantum chemical predictions of the frequencies in Table 1 both with and without anharmonic corrections. An additional column listing scaled harmonic frequencies from the B3LYP calculations is included which uses an empirical scaling factor (0.9679) derived following comparison of experimental and B3LYP predictions for a set of 125 small molecules.[38] The scaled harmonic values provide the best estimates (within 2%) for vibrations in the CH stretching and CH_2 bending regions above 1100 cm^{-1} as has been noted for other heterocycles.[35] The anharmonic-corrected frequencies from both the B3LYP and MP2 methods perform nearly as well in this region but at a substantial extra computational cost, requiring ~80 to 250 times longer to complete for these two methods respectively. In the far IR region, the B3LYP level estimates are more accurate than their MP2 counterparts, however, neither anharmonic corrections nor empirical scaling provides a systematic improvement over the rapid B3LYP harmonic calculations. For the lowest frequency ring puckering mode at 53 cm^{-1}, the harmonic calculations overestimate the frequency by 25% and the anharmonic terms increase the discrepancy to nearly 90%. For comparison, the ring puckering mode of silacyclobutane (158 cm^{-1}) is described by a deeper double-well

potential with barrier to planarity (440 cm^{-1}) above the lowest vibrational levels and in this case, the frequency is predicted to within 7.5% (146 cm^{-1}) using harmonic calculations at the B3LYP/6-311++(2d,2p) level with the anharmonic terms providing a slightly worse estimate (142 cm^{-1}) but still within 10%.[12] For a more harmonic potential, such as that of 3-oxetanone (with only a small quartic term in the potential), the level of agreement with experiment for the ring puckering mode (140 cm^{-1})[39] is similar with the harmonic calculations matching within 6.4% (149 cm^{-1} harmonic) and the anharmonic corrections predicting the value to within 13% (158 cm^{-1} anharmonic) at the B3LYP/6-311++(2d, 3p) level).[35] The quantum chemical results for TMO in this work are far less accurate and demonstrate that generic corrections are insufficient for modeling the low frequency modes of molecules with large amplitude motions and that in such cases, a more detailed theoretical treatment is needed.

6. Conclusions

Herein, we have described the rovibrational analysis of the C-O asymmetric stretch (ν_{23}) of TMO at 1008 cm^{-1} as well as two of its hotbands which originate in excited ring puckering states (ν_{18}, $2\nu_{18}$). Loomis-Wood plots clearly showed the presence of perturbations in the transitions of the ν_{23} band which necessitated analysis of the rovibrational structure of the overlapping C-C symmetric stretch at 1033 cm^{-1} which couples through a second order *c-type* Coriolis interaction. Another perturbation arises from interactions with a lower energy "dark" state which we assert is most likely due to a combination of energy levels from ring puckering and C-C asymmetric stretching ($\nu_{18}+\nu_{24}$) around 997 cm^{-1}. In the end, we could account for nearly 4400 transitions involving eight

different vibrational states in the frequency range from 960-1060 cm^{-1}. The spectroscopic parameters derived in the course of this work will be useful for analyzing the dense rotationally-resolved spectrum of TMO between 700 - 950 cm^{-1}. Based on preliminary rovibrational assignment of bands in this region, we have identified inconsistencies in the previous assignments of fundamental modes but thorough analysis will require treatment of multiple perturbations in a similar fashion to what we have described above. The current work has laid important ground work for theoreticians and experimentalists to continue to improve models of the lowest energy states of floppy molecules like TMO.

Acknowledgments

Supplementary data

A complete listing of the assigned rovibrational transitions is provided as supplementary information.

References

(1)   Legon, A. C. Equilibrium Conformations of Four- and Five-Membered Cyclic Molecules in the Gas Phase: Determination and Classification. *Chem. Rev.* **1980**, *80* (3), 231–262.
(2)   Laane, J. Spectroscopic Determination of Ground and Excited State Vibrational Potential Energy Surfaces. *Int. Rev. Phys. Chem.* **1999**, *18* (2), 301–341.
(3)   Fernandez, J.; Myers, R. J.; Gwinn, W. D. Microwave Spectrum and Planarity of

the Ring of Trimethylene Oxide. *J. Chem. Phys.* **1955**, *23* (4), 758–759.

(4)   Chan, S. I.; Zinn, J.; Fernandez, J.; Gwinn, W. D. Trimethylene Oxide. I. Microwave Spectrum, Dipole Moment, and Double Minimum Vibration. *J. Chem. Phys.* **1960**, *33* (6), 1643–1655.

(5)   Chan, S. I.; Borgers, T. R.; Russell, J. W.; Strauss, H. L.; Gwinn, W. D. Trimethylene Oxide. III. Far-Infrared Spectrum and Double-Minimum Vibration. *J. Chem. Phys.* **1966**, *44* (3), 1103–1111.

(6)   Jokisaari, J.; Kauppinen, J. Vapor-Phase Far-Infrared Spectrum and Double Minimum Potential Function of Trimethylene Oxide. *J. Chem. Phys.* **1973**, *2260* (May 2013), 2260–2263.

(7)   Harris, D. O.; Harrington, H. W.; Luntz, A. C.; Gwinn, W. D. Microwave Spectrum, Vibration-Rotation Interaction, and Potential Function for the Ring-Puckering Vibration of Trimethylene Sulfide. *J. Chem. Phys.* **1966**, *44* (9), 3467–3480.

(8)   Laane, J.; Lord, R. C. Far-Infrared Spectra of Ring Compounds. III. Spectrum, Structure, and Ring-Puckering Potential of Silacyclobutane. *J. Chem. Phys.* **1968**, *48* (4), 1508–1513.

(9)   van Wijngaarden, J.; Desmond, D.; Leo Meerts, W. Analysis of High Resolution FTIR Spectra from Synchrotron Sources Using Evolutionary Algorithms. *J. Mol. Spectrosc.* **2015**, *315*.

(10)   Pringle, W. C. Microwave Spectrum, Vibration-Rotation Interaction, and Ring Puckering Vibration in Silacyclobutane and Silacyclobutane-1,1-D2. *J. Chem. Phys.* **1971**, *54* (12), 4979–4988.

(11)   van Wijngaarden, J.; Chen, Z.; van Dijk, C. W. C. W.; Sorensen, J. L. J. L. Pure Rotational Spectrum and Ring Inversion Tunnelling of Silacyclobutane. *J. Phys. Chem. A* **2011**, *115* (31), 8650–8655.

(12)   Chen, Z.; van Wijngaarden, J. Synchrotron-Based Far Infrared Study of the Rotation-Vibration-Inversion Spectrum of Silacyclobutane below 500 cm^{-1}: The ν_{29} and ν_{30} Bands. *J. Chem. Phys.* **2013**, *139* (24).

(13)   Chen, Z.; van Wijngaarden, J. Analysis of the Rotation-Vibration-Inversion Infrared Spectrum of the ν_{10} and ν_{14} Bands of Silacyclobutane. *J. Mol. Spectrosc.* **2015**, *307*.

(14)   López, J. C.; Lesarri, A. G.; Alonso, J. L.; Spiehl, R.; Guarnieri, A. The Millimetre-Wave Spectrum of Trimethylene Sulphide Vibration-Rotation Coupling between the V=2 and V=3 Ring-Puckering Excited States. *Mol. Phys.* **1994**, *82* (2), 283–302.

(15)   Creswell, R. A.; Mills, I. M. Microwave Spectra and Centrifugal Distortion Constants of Oxetane. *J. Mol. Spectrosc.* **1974**, *52* (3), 392–412.

(16)   Creswell, R. A. Molecular Structure of Oxetane. *Mol. Phys.* **1975**, *30* (1), 217–222.

(17)   Lesarri, A.; Blanco, S.; López, J. C. The Millimetre-Wave Spectrum of Oxetane. *J. Mol. Struct.* **1995**, *354* (3), 237–243.

(18)   Danti, A.; Lafferty, W. J.; Lord, R. C. Far Infrared Spectrum of Trimethylene Oxide [1]. *J. Chem. Phys.* **1960**, *33* (1), 294–295.

(19)   Winnewisser, M.; Kunzmann, M.; Lock, M.; Winnewisser, B. P. The High-Resolution FIR-Spectrum of Oxetane. *J. Mol. Struct.* **2001**, *561* (1–3), 1–15.

(20)   Moruzzi, G.; Kunzmann, M.; Winnewisser, B. P.; Winnewisser, M. Ritz

Assignment and Watson Fits of the High-Resolution Ring-Puckering Spectrum of Oxetane. *J. Mol. Spectrosc.* **2003**, *219* (1), 152–162.

(21) Zürcher, R. F.; Günthard, H. H. Schwingungsspektren Und Thermodynamische Eigenschaften. *Helv. Chim. Acta* **1955**, *6634* (1953).

(22) Wieser, H.; Danyluk, M.; Kiefer, W.; Bernstein, H. J. Scissoring Region and the Ring Puckering Vibration of Trimethylene Oxide and Some Deuterated Analogs. *Can. J. Chem.* **1972**, *50* (17), 2771–2775.

(23) Wieser, H.; Danyluk, M. Infrared Band Progressions in the CH2 Scissoring Region and the Ring Puckering Vibration of Trimethylene Oxide and Some Deuterated Analogs. *Can. J. Chem.* **1972**, *50* (17), 2761–2770.

(24) Wieser, H.; Danyluk, M.; Kydd, R. A.; Kiefer, W.; Bernstein, H. J. Vibrational Spectra and Ring Puckering Progressions in the C-H Stretching Region of Trimethylene Oxide and Several Deuterated Analogs. *J. Chem. Phys.* **1974**, *61* (11), 4380–4393.

(25) Ueda, T.; Shimanouchi, T. Near-Infrared Band Progressions of Ring Molecules and Ring-Puckering Motion. *J. Chem. Phys.* **1967**, *47* (12), 5018–5030.

(26) Kydd, R. A.; Wieser, H.; Kiefer, W. Vibrational Assignments for Trimethylene Oxide and Several Deuterated Analogues. *Spectrochim. Acta Part A Mol. Spectrosc.* **1983**, *39* (2), 173–180.

(27) Green, W. H. Ring-Puckering Data from the Mid-infrared. *J. Chem. Phys.* **1970**, *52* (4), 2156–2157.

(28) Sellers, H.; Almlöf, J.; Saebø, S.; Pulay, P. Ring Puckering Potential of Oxetane: TZ + NP/MP4 (SDQ) Results. *J. Phys. Chem.* **1987**, *91* (16), 4216–4218.

(29) Bánhegyi, G.; Pulay, P.; Fogarasi, G. Ab Initio Study of the Vibrational Spectrum and Geometry of Oxetane-I. Interpretation of the Vibrational Spectra. *Spectrochim. Acta Part A Mol. Spectrosc.* **1983**, *39* (9), 761–769.

(30) Foltynowicz, I. Theoretical Calculations of the Ring-Puckering Vibration for Trimethylene Oxide (TMO) and Its Deuterated Derivatives. The Semirigid Models for the Large-Amplitude Ring-Puckering Vibration. *J. Mol. Spectrosc.* **1982**, *96* (2), 239–246.

(31) McKellar, A. R. W. High-Resolution Infrared Spectroscopy with Synchrotron Sources. *J. Mol. Spectrosc.* **2010**, *262* (1), 1–10.

(32) Tokaryk, D. W.; van WijngaardenJ.A. Fourier Transform Spectra of the ν_{16}, $2\nu_{16}$, and $2\nu_{16}$-ν_{16} Bands of Pyrrole Taken with Synchrotron Radiation. *Can. J. Phys.* **2009**.

(33) Frisch, M. J.; Trucks, G. W.; Schlegel, H. B.; Scuseria, G. E.; Robb, M. A.; Cheeseman, J. R.; Scalmani, G.; Barone, V.; Mennucci, B.; Petersson, G. A.; et al. Gaussian 09, Revision B.01. Gaussian, Inc., Wallingford CT. 2010.

(34) Chen, Z.; van Wijngaarden, J. A Combined Ab Initio, Fourier Transform Microwave and Fourier Transform Infrared Spectroscopic Investigation of β-Propiolactone: The ν_8 and ν_{12} Bands. *J. Mol. Spectrosc.* **2009**, *257* (2).

(35) Chen, Z.; van Wijngaarden, J. Synchrotron-Based Far-Infrared Spectroscopic Investigation and Ab Initio Calculations of 3-Oxetanone: Observation and Analysis of the ν_7 Band and the Coriolis Coupled ν_{16} and ν_{20} Bands. *J. Phys. Chem. A* **2012**, *116* (38).

(36) Igor Pro Version 6.03A. https://www.wavemetrics.com (accessed Apr 21, 2020).

(37) Pickett, H. M. The Fitting and Prediction of Vibration-Rotation Spectra with Spin Interactions. *J. Mol. Spectrosc.* **1991**, *148* (2), 371–377.

(38) Andersson, M. P.; Uvdal, P. New Scale Factors for Harmonic Vibrational Frequencies Using the B3LYP Density Functional Method with the Triple-ζ Basis Set 6-311+G(d,P). *J. Phys. Chem. A* **2005**, *109* (12), 2937–2941.

(39) Chen, Z.; van Wijngaarden, J. The ν_{21} Ring Puckering Mode of 3-Oxetanone: A Far Infrared Spectroscopic Investigation Using Synchrotron Radiation. *J. Mol. Spectrosc.* **2012**, *279* (1).

TOC Graphic